J Mater Sci: Mater Electron (2020) 31:17524–17534

Synthesis of novel ternary $Bi_2WO_6/CeO_2/g\text{-}C_3N_4$ composites with enhanced visible light photocatalytic activity for removal of organic and Cr(VI) from wastewater

Yichen Bai[1,2], Tianye Wang[1,2], Xinyu Zhao[3], Wei Mao[3], and Shuxia Liu[1,2,*]

[1] College of Resources and Environment, Jilin Agricultural University, Changchun 130000, China
[2] Key Laboratory of Soil Resource Sustainable Utilization for Jilin Province Commodity Grain Bases, Changchun 130118, China
[3] Guangdong Provincial Engineering Technology Research Center for Urban Water Cycle and Water Environment Safety, Graduate School at Shenzhen, Tsinghua University, Shenzhen 518055, China

Received: 19 November 2019
Accepted: 21 August 2020
Published online: 8 September 2020

ABSTRACT

In this study, novel ternary $Bi_2WO_6/CeO_2/g\text{-}C_3N_4$ composites were synthesized successfully in this study, which exhibited enhanced visible-light photocatalytic activity for oxidization of rhodamine B (RhB) and tetracycline hydrochloride (TH) as well as reduction of Cr(VI). The characteristics of the as-prepared composites were investigated in detail by X-ray diffraction (XRD), Transmission Electron Microscopy (TEM), X-ray Photoelectron Spectroscopy (XPS), Scanning Electron Microscopy (SEM), Fourier Transform Infrared spectra (FT-IR), UV–vis diffuse reflectance spectra (UV-DRS), Photoluminescence spectra (PL), Electrochemical Impedance Spectroscopy (EIS) and Mott-Schottky curves. The results demonstrated that the ternary heterojunctions were formed between Bi_2WO_6, CeO_2 and $g\text{-}C_3N_4$, which can narrow the band gap to improve separation and migration of photogenerated electrons-hole pairs, so that the lifetimes of photogenerated charge carriers were prolonged to involve in photocatalytic reaction. Therefore, $Bi_2WO_6/CeO_2/g\text{-}C_3N_4$ can generate abundant free radicals under visible-light irradiation to enhance photocatalytic activity. BW/Ce/g-3 can degrade 99.24% of RhB in 75 min and 54.76% of TH in 105 min. More than that, BW/Ce/g-3 exhibited enhanced photocatalytic reduction for Cr(VI) (94.85%, 30 min). Meanwhile, the best synthesized condition was determined that the adding amount of CeO_2 was 0.043 g and $g\text{-}C_3N_4$ was 0.02 g. This study not only provided a mothed to synthesize $Bi_2WO_6/CeO_2/g\text{-}C_3N_4$ ternary

Yichen Bai and Tianye Wang contributed equally to this work and should be considered co-first authors.

Address correspondence to E-mail: liushuxia69@163.com

https://doi.org/10.1007/s10854-020-04308-4

heterojunctions, but also confirmed a photocatalyst for degrading both organic pollution and heavy metals wastewater.

1 Introduction

Treatments of dye wastewater and pharmaceutical wastewater are hard for traditional sewage treatment technology, because these kinds of organic contaminants are high molecular weight and trace amount in the environment [1, 2]. Not only that, heavy metals pollution always coexist in organic wastewater, such as Cr(VI), which is another crucial issue in sewage treatment technology [1]. This kind of heavy metals with high toxicity and high solubility has been confirmed to cause serious harm to the aquatic creatures and environments, even taking for mutagenic and carcinogenic risks to animals and human [3]. Hence, it is highly meaningful to find an effective advances wastewater technologies to degrade organic pollutants and reduce Cr(VI) simultaneously [1].

Semiconductor photocatalysis has emerged as one of the most promising technologies for environmental remediation and solar energy conversion [4], which is considered as one of the most appealing and promising technologies in environmental purification [5]. Realization of efficient absorption and utilization of the visible light in solar energy is extremely essential for improving the photocatalytic properties of photocatalyst [6]. Hence, it is still highly crucial to explore novel visible-light photocatalysts with great photodegradation performance [4]. This type of novel photocatalysts not only have narrow band gaps to facilitate the immigration of photogenerated electrons, but also possess stable structures and conductive to inhibit recombination of photogenerated hole-electron pairs [7].

With the extensive and in-depth of exploration of novel photocatalysts, combining more than two kinds of materials is one of the most effective ways to synthesize novel semiconductor photocatalysts. Among the selected materials, bismuth tungstate (Bi_2WO_6) and Ceria (CeO_2) have attracted a great deal of attention [8, 9]. Because Bi_2WO_6 possesses excellent intrinsic physical and chemical properties, such as nonlinear dielectric susceptibility and photocatalytic activity [10], as well as that CeO_2 has unique ultraviolet absorbing ability, high mass density, low thermal expansion, low phonon energy and good chemical stability [9]. Furthermore, Bi_2WO_6 and CeO_2 have been adopted to synthesized novel photocatalysts that exhibited visible-light photocatalytic activity [8, 11, 12].

Not only that, among tremendous novel materials, the layered graphitic carbon nitride (g-C_3N_4) as a typical metal-free semiconductor has been widely reported to be adopted in synthesis of novel photocatalysts due to low cost, stable chemical structure and strong visible-light absorption [13, 14]. Hence, g-C_3N_4 are usually adopted to combine with other materials to synthesize novel photocatalysts with high photodegradation performance [15]. Bi_2WO_6 has been loaded on g-C_3N_4, this composite showed well photocatalytic activity and photoreducibility [16–18]. In addition, it also has been reported that CeO_2 combining with g-C_3N_4 possessed great photodegradation for organic wastes and photoreducibility for CO_2 reduction and hydrogen evolution [13, 19, 20]. Although some articles including Bi_2WO_6, CeO_2, g-C_3N_4 have been reported, there is not article involved the ternary Bi_2WO_6/CeO_2/g-C_3N_4 composites, as well as that the photocatalytic performance has clarified.

In order to further increase visible-light response ability and photodegradation performance for various contaminants, it is the first time to designed Bi_2WO_6, CeO_2 and g-C_3N_4 to synthesize a novel ternary Bi_2WO_6/CeO_2/g-C_3N_4 composites. More than that, both of visible-light photooxidation and photoreduction performance over the as-prepared composites were clarified via photodegradation of dye wastewater (RhB), pharmaceutical wastewater (tetracycline hydrochloride) and heavy metal wastewater (Cr(VI)). In addition, the mechanisms of the highly efficient photocatalytic activity over ternary Bi_2WO_6/CeO_2/g-C_3N_4 composites will be probed through various characterizations methods. This study not only confirms the feasibility of formation of ternary Bi_2WO_6/CeO_2/g-C_3N_4 composites with enhanced photocatalytic activity, but also provides a novel photocatalyst for simultaneously effective degradation of organic wastewater and heavy metals wastewater.

2 Experiments and methods

2.1 Synthesis methods

Synthesis of CeO_2: 0.05 mol $Ce(NO_3)_3$ was added to 0.1 L distilled water, stirring until it dissolved, and then 0.015 mol NH_4NO_3 was added the solution immediately. After dissolution, 0.016 mol NH_4HCO_3 was injected into the mixed solution evenly at room temperature. The mixture was deposited for aging at 80 °C for 4 h. After cooling, the precipitate was dried in an drying oven at 60 °C for 12 h. Finally, the precursor was calcined in a muffle furnace at 500 °C for 2 h. After cooling, CeO_2 were ground to prepare for the next experiment.

Synthesis of g-C_3N_4: the method was same with that our research group has published previously [17].

Synthesis of Bi_2WO_6/CeO_2/g-C_3N_4: 4 mmol $Bi(NO_3)_3{\cdot}5H_2O$ was dissolved into 35 mL mixed solution of 4 mmol solution of sodium oleate and ethylene glycol. At the same time, 2 mmol $Na_2WO_4{\cdot}2H_2O$ was dissolved into 20 mL ethylene glycol. And then, the two solutions were mixed, stirring for 1 h. A certain amount of CeO_2 and 0.02 g g-C_3N_4 was dissolved ultrasonically in 10 mL ethylene glycol for 30 min, respectively. Firstly, the CeO_2-ethylene glycol was injected into the above precursor solution of Bi_2WO_6, stirring for 1 h. Nest, g-C_3N_4-ethylene glycol was injected into this mixture solution, stirring for 2 h. And then, the precursor mixtures were sealed in a 100 mL Teflon-lined autoclave and heated at 180 °C for 20 h. After cooling to the room temperature, the mixtures were washed and filtered with mixed solution of distilled water and ethylene glycol, drying at 60 °C for 12 h. Finally, the mixtures were ground to obtain the black powdered Bi_2WO_6/CeO_2/g-C_3N_4 (abbreviated as BW/Ce/g). The added amount of CeO_2 corresponding to the sample numbers were 0.344 g for BW/Ce/g-1; 0.172 g for BW/Ce/g-2; 0.086 g for BW/Ce/g-3; 0.043 g for BW/Ce/g-4, separately. Meanwhile, for comparison, pure Bi_2WO_6 (abbreviated as BW) was synthesized under the same consideration.

2.2 Characterization

X-ray diffractometry (XRD) was conducted using a Japan Rigaku Rotaflex diffractometer with a monochromatic Cu Kα radiation source, under 40 kV and 100 mA (λ = 0.15418 Å). Transmission electron microscopy (TEM) was recorded on a FECNAI F20 microscope. Energy-dispersive X-ray spectroscopy (EDS) was additionally conducted during TEM measurement. Scanning electron microscopy (SEM) images were observed by a JEOLJSM-6700F SEM device. X-ray photoelectron spectroscopy (XPS) measurement performed in an ESC ALAB-250I-XL device, which take a monochromatic Al target X-ray source (hv = 1486.6 eV) and a DLD detector, the binding energy was adjusted by carbon C1s (284.60 eV). Fourier transform infrared spectra (FT-IR) were undertaken in a Nicolet 500 FT-IR analyzer in the region 4000–400 cm^{-1} and using KBr pellets. Ultraviolet–visible diffuse reflectance spectra (UV-DRS) were recorded by a Shimada (Japan) UV-2550 spectrometer using $BaSO_4$ as a reference. Photoluminescence (PL) spectra were measured at room temperature on a Hitachi F-4600 fluorescence spectrophotometer (λEx = 338 nm). Electrochemical impedance spectroscopy (EIS) and Mott–Schottky curves of thin films of the prepared materials were performed on a computer-controlled in a conventional three-electrode, single-compartment quartz cell on an electrochemical workstation (CHI-600E) under A 100 W LED cold lamp. EIS measurements were carried out in 0.5 M Na_2SO_4 solution at an open circuit potential over a frequency range from 10^5 to 10^{-2} Hz. Mott–Schottky plots were measured at frequencies of 1000 Hz in 0.5 M Na_2SO_4 solution.

2.3 Photocatalytic activity

Photocatalytic activities of BW/Ce/g were evaluated through the photodegradation of Rhodamine B and tetracycline hydrochloride under the irradiation of a 500 W Xe lamp in a sealed photocatalytic reactor. Firstly, 0.01 g of the as-prepared photocatalysts were added to a 0.1 L RhB solution (0.01 g/L) or TH solution (0.01 g/L) or Cr(VI) solution (0.01 g/L). The solution was stirred for 75 min in the dark to reach adsorption–desorption equilibrium before irradiation. After that, the mixture solution encompassing the photocatalysts and the tested solution were situated below the Xe lamp. As for RhB and TH, a 0.0035 L aliquot was sampled at each 15 min interval, meanwhile, centrifuged to discard the photocatalyst particles, as for Cr(VI) at 5 min interval. Next, the absorbance of the centrifuged solution was measured at 553 nm for RhB or 357 nm for TH or 540 nm for

Cr(VI) in a Persee (Beijing) UV–visible spectrophotometer (TU-1901). Among them, the concentration of Cr(VI) was tested using the 1,5-diphenylcarbazide method [21].

3 Results and discussion

3.1 Characterization

The phase and composition of the as-prepared composites were characterized by XRD, as shown in Fig. 1. It can be found clearly that the diffraction peaks of the as-prepared composites can be indexed to the standard phase-pure orthorhombic Bi_2WO_6 (JCPDS No. 39-0256) [22], which implied that Bi_2WO_6 was synthesized in the solvothermal process. Meanwhile, the diffraction peaks were also able to correspond to the cubic fluorite-type CeO_2 (JCPDS No. 43-1002). Furthermore, there are more peaks corresponding to the characteristic peak of CeO_2 in BW/Ce/g-1 and BW/Ce/g-2 with the high amounts of CeO_2. It can be preliminarily indicated that the composites including Bi_2WO_6 and CeO_2 were synthesized. However, there was not g-C_3N_4 detected, which could be attributed to the few amounts of g-C_3N_4 [17].

TEM and HRTEM of BW/Ce/g-3 were displayed in Fig. 2, illustrating the morphologies and microstructures. It can be showed that BW/Ce/g has been synthesized to form nanoparticles (Fig. 2a). Additionally, the polycrystalline structure and high crystallinity of BW/Ce/g-3 can be determined by the diffraction rings of the selected area electron-diffraction pattern (inset in Fig. 2a) [6]. Furthermore, it can be observed there were four sets of lattice fringes (Fig. 2b). The lattice distance of 0.272 nm was corresponded to the (200) crystal plane of Bi_2WO_6 [23]. In addition, 0.312 nm d-spacing and 0.246 nm d-spacing were consistent with the (111) crystal plane and the (200) crystal plane of CeO_2, respectively. More than that, the 0.327 nm d-spacing representing the (002) plane of g-C_3N_4 was illustrated, which can demonstrate that g-C_3N_4 existed in these composites [24]. Moreover, the multiphase lattices and the polycrystalline structure can be suggested that the heterojunctions between Bi_2WO_6, CeO_2 and g-C_3N_4 were formed [25]. Meanwhile, Bi, W, C, N, O and Ce can be found as the major elements of BW/Ce/g-3 via EDS elemental microanalysis, which can further demonstrate the composites were synthesized by Bi_2WO_6, CeO_2 and g-C_3N_4. In short, the formation of heterojunctions between Bi_2WO_6, CeO_2 and g-C_3N_4 has been firmed by the results of TEM and EDS. The heterojunctions structure would imply that Bi_2WO_6/CeO_2/g-C_3N_4 owned a narrowed band gap, so that the electrons can be departed from holes and transfer into the conduction band more easily under the visible-light irradiation.

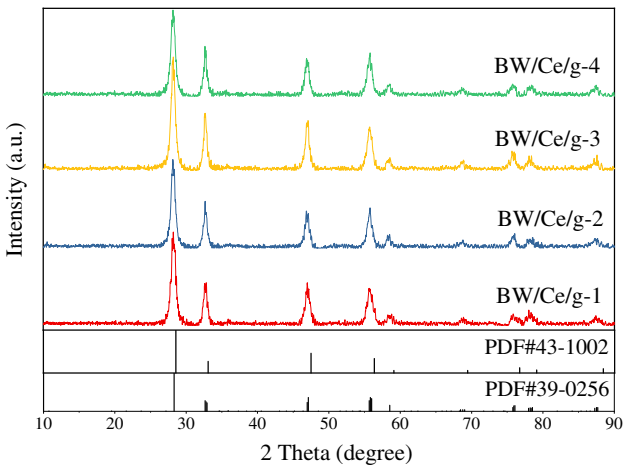

Fig. 1 XRD patterns of the as-prepared composites

XPS spectra of BW/Ce/g-3 were displayed in Fig. 3, which was adopted to analyze the surface element composition and the chemical states of all the elements in the as-prepared composites. Among them, the peaks of Bi 4f in BW/Ce/g-3 at two peaks 158.94 eV and 164.4 eV were representing to Bi $4f_{7/2}$ and Bi $4f_{5/2}$ spin states of Bi_2WO_6 [26, 27] (Fig. 3a). In addition, the peaks of W 4f in BW/Ce/g-3 at 35.1 eV and 37.5 eV were ascribed to W $4f_{5/2}$ and W $4f_{7/2}$, on behalf of W^{6+} in Bi_2WO_6 [23] (Fig. 3b). However, compared with the counterparts in Bi_2WO_6, some peaks representing Bi and W in BW/Ce/g-3 shifted, which implied the combination between Bi_2WO_6 and other materials via the change of these bond energy. Furthermore, Ce XPS spectra revealed that spectral peaks of Ce 3d were divided to v_0, v, v_1, v_2, v_3, u, u_1, u_2 and u_3 (Fig. 3c), which indicate the spin–orbit coupling of $3d_{5/2}$ and $3d_{3/2}$, respectively [28]. Among of them, the peaks located at v, v_2 and v_3 were attributed to $Ce^{4+}3d_{5/2}$, and the peaks located at u, u_2 and u_3 were assigned to $Ce^{4+}3d_{3/2}$, besides, the doublet peak of v_0, v_1 and u_1 represented Ce^{3+} $3d_{5/2}$ and $3d_{3/2}$ [6, 29]. But, compared with CeO_2, the v_0 peak of BW/Ce/g-3 disappeared and the v peak shifted left to low energy, as well as that the

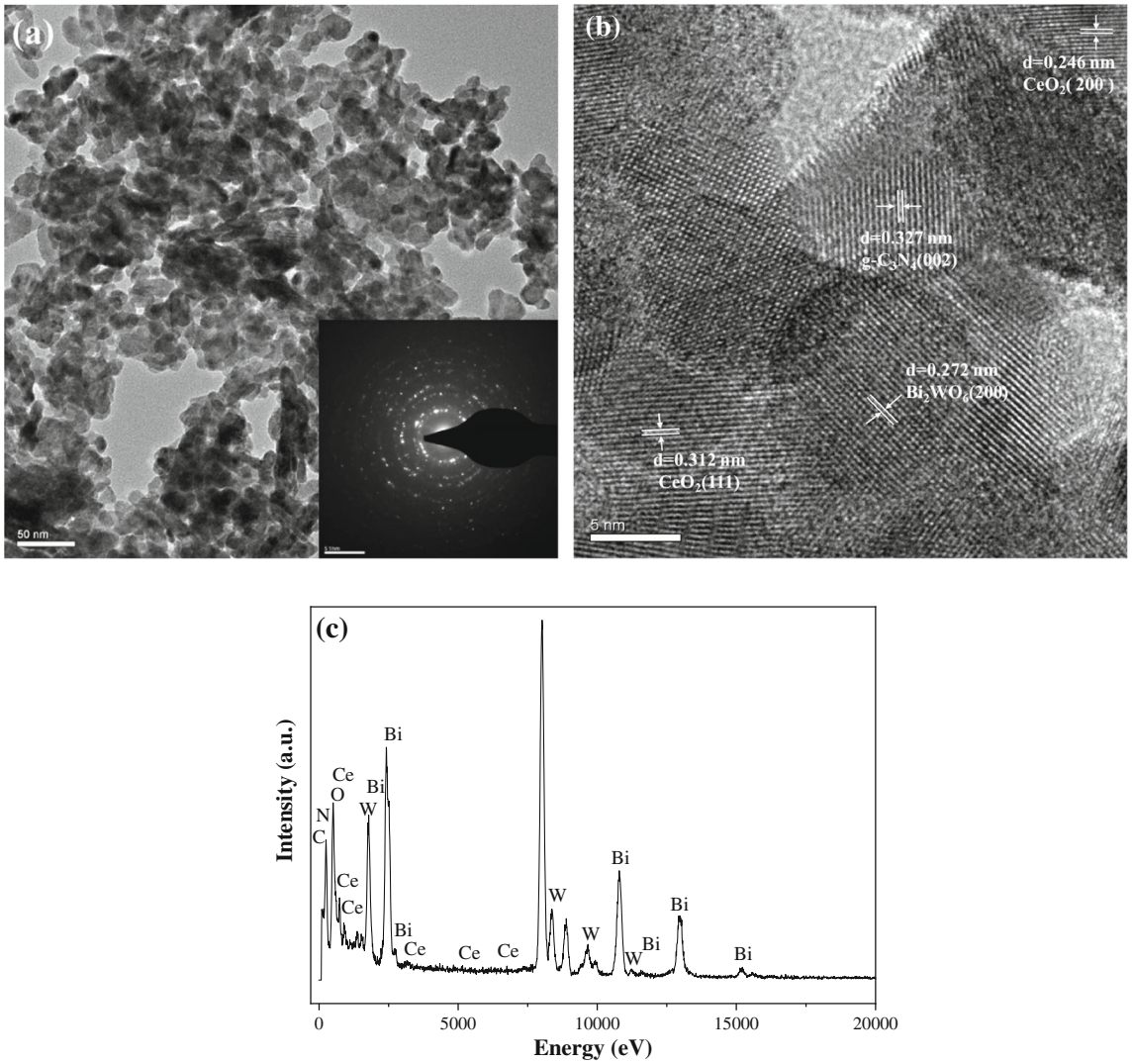

Fig. 2 TEM images and selected area electron diffraction (inset) (**a**), HRTEM micrographs of the lattice (**b**) and EDS spectra (**c**) of BW/Ce/g-3

intensities of the v_1 peak and the v_2 peak have changed, which meant the formation heterojunction between CeO_2 and other materials by changing of Ce^{3+}/Ce^{4+} bond [29]. Meanwhile, the peaks of O 1 s in CeO_2, g-C_3N_4 and BW/Ce/g-3 were showed differently (Fig. 3d). The peaks of O 1s in CeO_2 were represented the lattice oxygen (530.6 eV) and surface oxygen (533.1 eV) [30], the peaks of O1s (532.5 eV) in g-C_3N_4 represented organic carbon oxygen bonds [22], whereas the peaks of O 1s (530.8 eV) in BW/Ce/g-3 were on behalf of the crystal lattice oxygen of metallic oxides [31]. This can be indicated that all types of oxygen have been transformed into the more stable lattice oxygen during formation of heterojunctions. More than that, the peak of C 1s and N 1s on behalf of g-C_3N_4 have been changed as well. The peaks of C 1s in g-C_3N_4 at 284.8 and 288.3 eV were attributed to C–N and N–C=N of g-C_3N_4, respectively, nevertheless the peak in BW/Ce/g-3 at 284.8 eV was corresponded to the bond of C–N [32] (Fig. 3e). Likewise, the peaks of N1s in g-C_3N_4 at 395.5 eV and 397.2 eV were attributed to sp^2-hybridized nitrogen (C–N=C), and tertiary nitrogen N–(C3), respectively [33, 34], which has been shifted to the peak at 398.6 in BW/Ce/g-3 (Fig. 3f). The results of C 1s and N 1s meant that g-C_3N_4 coupled with other materials to form the heterojunctions via the shift of carbon–nitrogen bonds. Hence, integrated these results, not only the existence of CeO_2 and g-C_3N_4 in the as-prepared composites can be

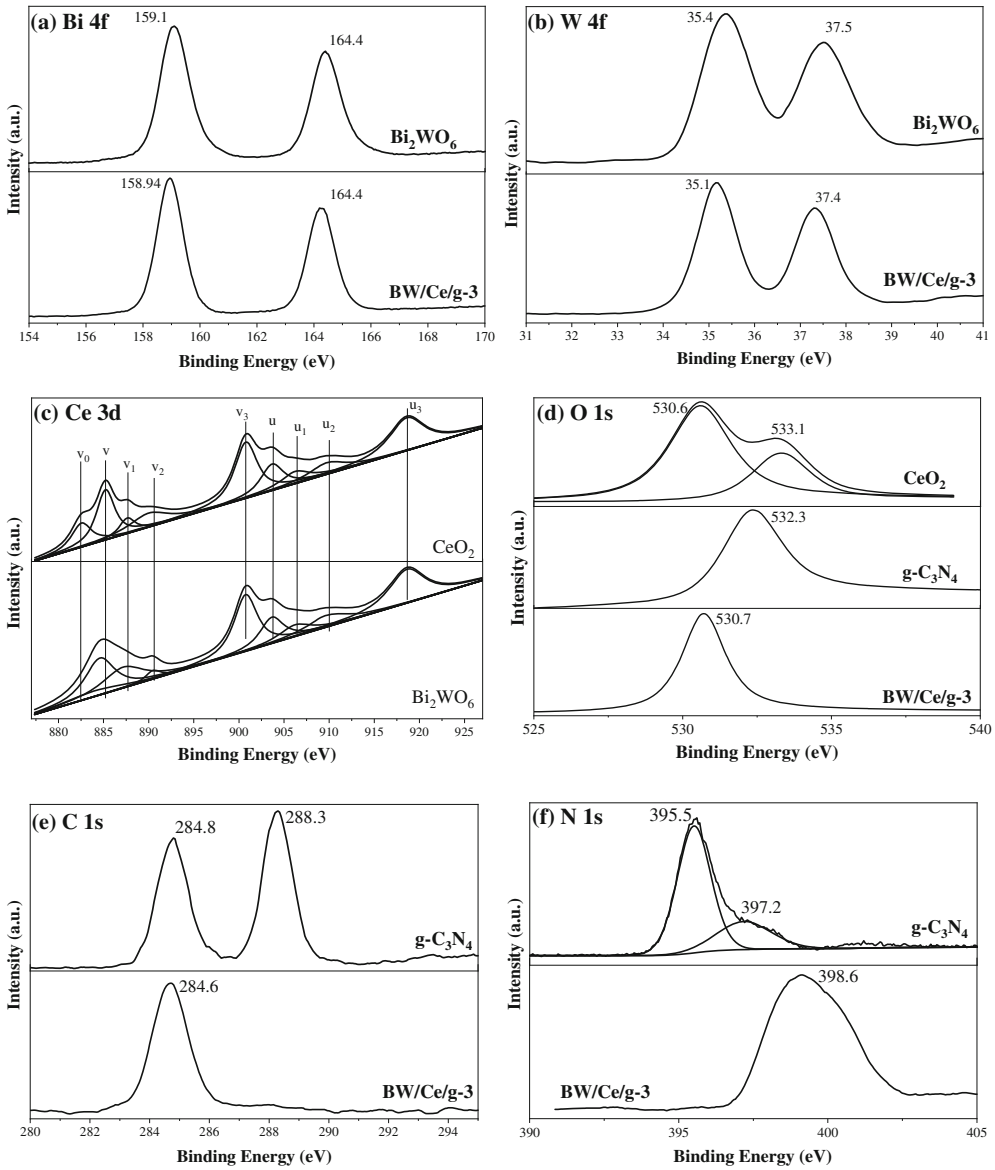

Fig. 3 XPS spectra of Bi 4f (**a**), W 4f (**b**), Ce 3d (**c**), O 1s (**d**), C 1s (**e**), N 1s (**f**)

furthermore confirmed, but also the formation of the ternary heterojunction was determined between CeO_2, g-C_3N_4 and Bi_2WO_6 by chemical change of bonds, as well as that the structure was more stable.

UV–vis diffuse reflectance of BW/Ce/g composites was shown in Fig. 4, investigating the visible-light response capability of the as-prepared composites to further suggest the potential of enhanced photocatalytic activity. It can be found that all the as-prepared composites possessed great absorbance in the UV–vis light region (Fig. 4a), especially within the visible-light region (400–800 nm). The result suggested that BW/Ce/g composites possessed well the visible-light response capability.

In addition, the Kubelka–Munk equation can be used to calculate the band gap energy of BW/Ce/g composites and Bi_2WO_6:

$$\alpha h\upsilon = A\left(h\upsilon - E_g\right)^{n/2} \quad (1)$$

where, α *is* the absorption coefficient, h is the Planck constant, υ *is* the light frequency, E_g is band gap, and A is a constant. Among them, n is determined from the type of optical transition of a semiconductor, so the value of n for the direct semiconductor (Bi_2WO_6) is 1 [35]. The band gaps were estimated from the

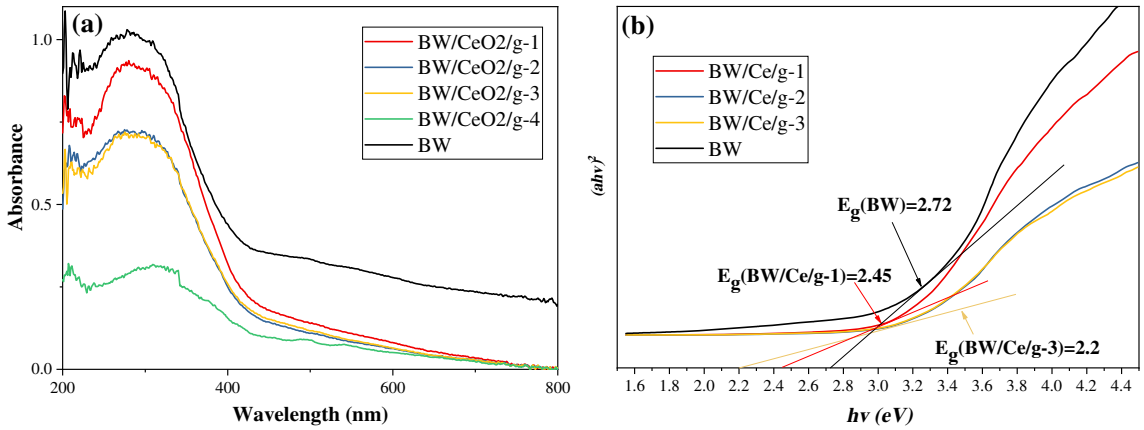

Fig. 4 **a** UV–vis diffuse reflectance spectra of BW/Ce/g; **b** band gaps of the as-prepared composites

$(\alpha hv)^2$ versus photon energy (hv) plots were approximately 2.2 eV (BW/Ce/g-3 and BW/Ce/g-2), 2.45 eV (BW/Ce/g-1) and 2.72 eV (BW) respectively, as shown in Fig. 4b. It can be determined that combining CeO_2 and g-C_3N_4 effectively narrow the gap band of BW/Ce/g composites, which was supposedly attributed to the heterojunction structure.

3.2 Photocatalytic activity

Photocatalytic activity of Bi_2WO_6/CeO_2/g-C_3N_4 for degrading RhB under visible-light irradiation was shown in Fig. 5a. It can be obviously demonstrated that BW/Ce/g-3 exhibited best photocatalytic activities, which degraded 99.24% of RhB in 75 min. Not only that, all the as-prepared composites showed better photocatalytic activities than that of Bi_2WO_6 after 60 min, even better than that of Bi_2WO_6/CeO_2 [11] and a similar Bi_2WO_6 composites [36]. Hence, it can be determined that combining CeO_2 and g-C_3N_4 can improve photocatalytic activity of Bi_2WO_6. This can be attributed to the formed heterojunction between Bi_2WO_6, CeO_2 and g-C_3N_4, which enable BW/Ce/g possessed enhanced visible-light response ability. Moreover, it was shown that the best as-prepared composite is BW/Ce/g-3. Consequently, BW/Ce/g-3 was chosen to be tested in the subsequent tests.

In order to further illustrate the photocatalytic activity of BW/Ce/g-3, the temporal progression of the spectra during the photodegradation for RhB under visible-light irradiation ($\lambda > 420$ nm) is presented in Fig. 5b. A quick decline of RhB absorption was detected at wavelength of 553 nm, and then the peak of the spectral maximum move from 553 to 496 nm. The hypsochromic shifts were likely induced by the release of N-ethyl groups and the elimination of the conjugated structure from RhB during photodegradation [37]. These results also demonstrate that the chemical structure of RhB was changed by

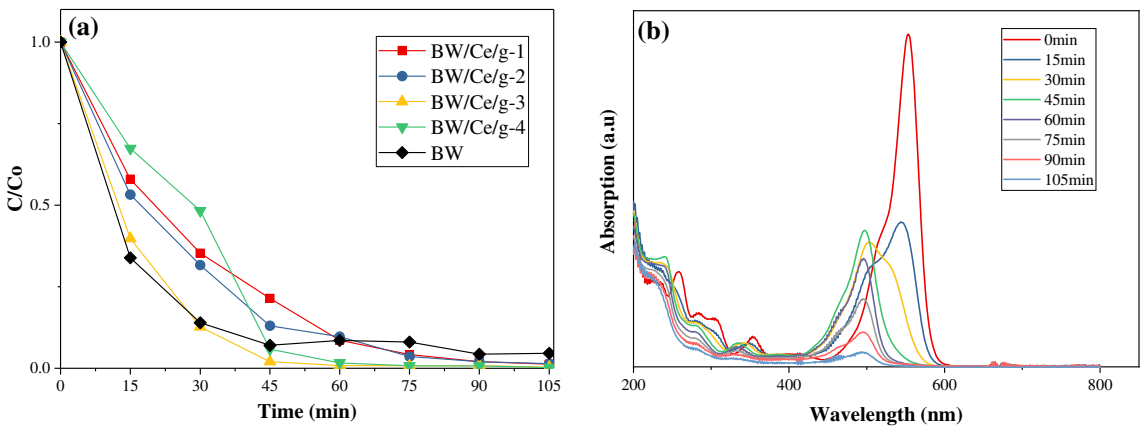

Fig. 5 **a** Photodegradation for RhB by the as-prepared composites **b** UV–vis spectra of the reaction solution with BW/Ce/g-3

the photocatalytic activity of BW/Ce/g during the degradation process, rather than adsorption. Overall, these results demonstrated that BW/Ce/g-3 displayed excellent photocatalytic activity for degrading RhB.

BW/Ce/g exhibited enhanced photocatalytic activity, not only for degrading dye wastewater, but also for degrading pharmaceutical and heavy metal wastewater, such as tetracycline hydrochloride and Cr(VI), as illustrated in Fig. 6. BW/Ce/g-3 can photodegrade TH to 54.76% in 105 min (Fig. 6a), which is better than 47.26% of Bi_2WO_6. In addition, it can be found that BW/Ce/g-3 did not show adsorption for TH, hence, it can be determined that degradation of TH was ascribed to the photocatalytic activity rather than adsorption ability.

Meanwhile, BW/Ce/g-3 exhibited excellent photoreduction for Cr(VI), reducing 94.85% of Cr(VI) in 30 min, compared to 38.46% of Bi_2WO_6 (Fig. 6b). It can be found that, compared with counterpart of enhancing photooxidation, combining CeO_2/g-C_3N_4 can improve photoreduction of Bi_2OW_6 more effectively. In addition, it can be found that BW/Ce/g-3 still owned a little reducing capacity in the absence of light. The excellent reducing capacity could be attributed to the g-C_3N_4, whose the CB position is relatively negative to facilitate the reduction ability of the photogenerated electrons [38]. Totally, these results can be further manifested that BW/Ce/g possessed highly effective photocatalytic activity not only for oxidized degradation of organic wastes, but also for reduction of heavy metals.

3.3 Possible photocatalytic mechanism

The separation efficiency of photogenerated electron–hole pairs of BW/Ce/g were assessed by photoluminescence spectra (excited at 370 nm), as shown in Fig. 8a. PL emissions are created from the radiative recombination of photogenerated electron–hole pairs. Hence, the higher PL emission indicates the easier recombination of charge carriers [39]. It can be found that PL emission peaks decreased with reducing amount of CeO_2. CeO_2 did not play the important role to inhibit the recombination of photogenerated electron–hole pairs as expected, instead the recombination was promoted with the increase of the addition amount. Hence, it would be deduced that g-C_3N_4 was the main reason to inhibit the recombination of the photogenerated electron–hole pairs.

In order to further clarify the effect of g-C_3N_4 on the separation and migration of photogenerated electron-holes of BW/Ce/g, the interface charge separation efficiency was investigated by electrochemical impedance spectroscopy under visible-light irradiation ($\lambda > 420$ nm), as displayed in Fig. 7b. The radius of each arc is characteristic of the charge transfer process at the corresponding electrode/electrolyte interface with a smaller radius corresponding with a lower charge transfer resistance [40]. The arc radius of g-C_3N_4 was much smaller than that of BW/Ce/g-3 and Bi_2WO_6, which implied g-C_3N_4 owned excellent charge transfer ability. More than that, the arc radius of BW/Ce/g-3 was smaller than that of Bi_2WO_6, suggesting that BW/Ce/g-3 exhibited a smaller charge transfer resistance than that of Bi_2WO_6 [41]. This result can be indicated that BW/Ce/g-3 would have more effective charge

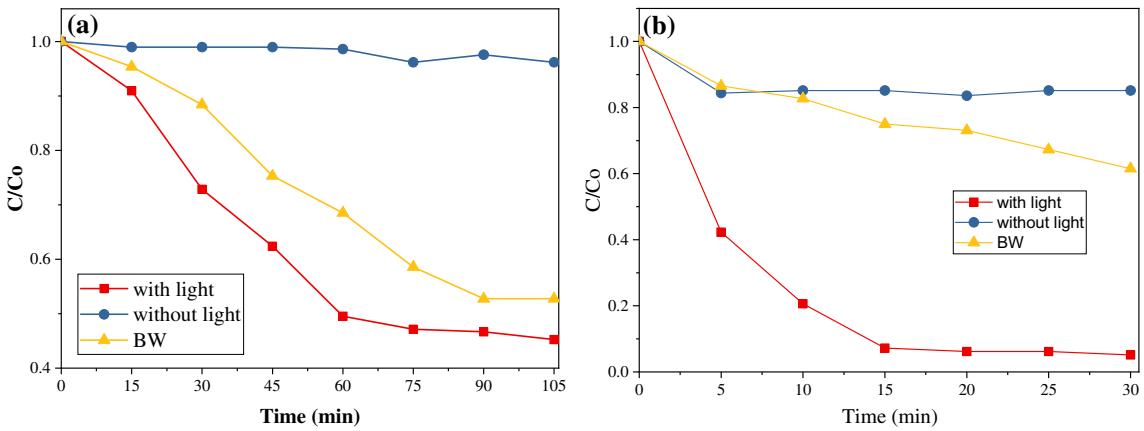

Fig. 6 Photodegradation for TH (**a**) and Cr(VI) (**b**) over BW/Ce/g-3

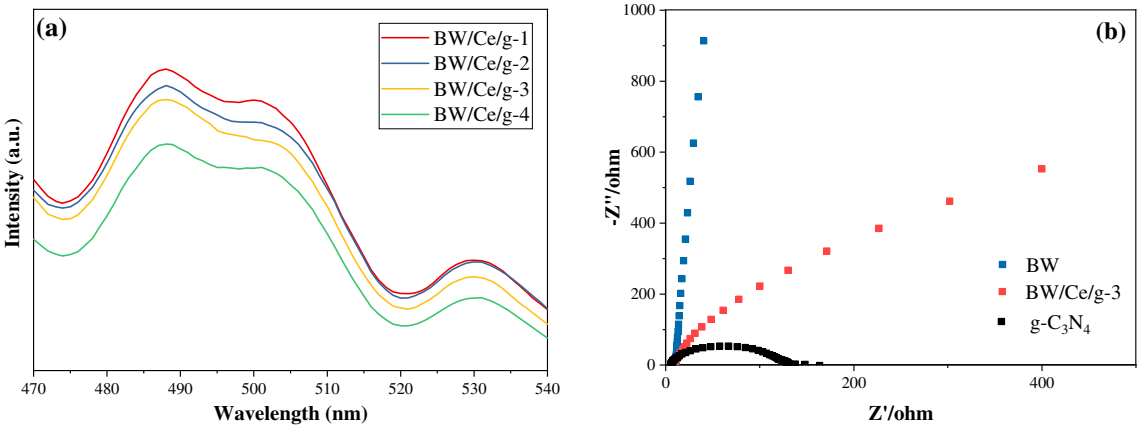

Fig. 7 **a** Room-temperature photoluminescence spectra of BW/Ce/g; **b** EIS Nyquist plots of BW/Ce/g-3, Bi_2WO_6 and g-C_3N_4

shuttling between the electrode and the electrolyte under coupling g-C_3N_4, therefore, a faster charges transfer can occur at the heterojunction interface between Bi_2WO_6, CeO_2 and g-C_3N_4 to enhance photocatalytic activity [10].

The band structure position of BW/Ce/g-3 was calculated by Mott-Schottky curves and depicted in Fig. 8, further elucidating a possible mechanism of the enhanced photocatalytic activity. On the basis of the Mott-Schottky equation, an observed positive slop indicated that BW/Ce/g-3 was n-type like semiconductors [42]. By extrapolation to $1/C^2 = 0$, the flat band position (V_{fb}) can be calculated as − 1.17 V (vs. Ag/AgCl electrode) and − 0.97 V (vs. NHE) for BW/Ce/g-3, − 1.76 V (vs. Ag/AgCl electrode) and − 1.56 V (vs. NHE) for Bi_2WO_6, − 1.48 (vs. Ag/AgCl electrode) and − 1.28 V (vs. NHE) for g-C_3N_4. Because the conduction band potential (C_{CB}) of the n-type semiconductor was very close to the NHE value of V_{fb} [43], the C_{CB} values of BW/Ce/g-3, Bi_2WO_6 and g-C_3N_4 were approximately − 0.97 V, − 1.56 V and − 1.28 V, separately. Integrated the estimated band gap energy of 2.2 eV (BW/Ce/g-3) and 2.72 eV (BW), as well as 2.7 eV for g-C_3N_4 and 2.83 eV for CeO_2 [44], the valence band positions (V_{VB}) of were determined as 1.23 V for BW/Ce/g-3, 1.16 V for pure Bi_2WO_6, 1.42 V for g-C_3N_4. Hence, the positions of the V_{VB} and the C_{CB} of BW/Ce/g was illustrated in Scheme 1.

The mechanism on charge separation in visible-light irradiation and enhanced photocatalytic activity of BW/Ce/g is illustrated in Scheme 1. Based on the above results, it can be determined that Bi_2WO_6 can couple with CeO_2 and g-C_3N_4 to construct the ternary heterojunctions structure, an interlaced energy level structure was formed, thus the band gap that the photogenerated electrons will transfer can be narrowed effectively. That means that electrons can be irritated more easily by visible light to departed from holes and transfer into the C_{CB}, which enable BW/

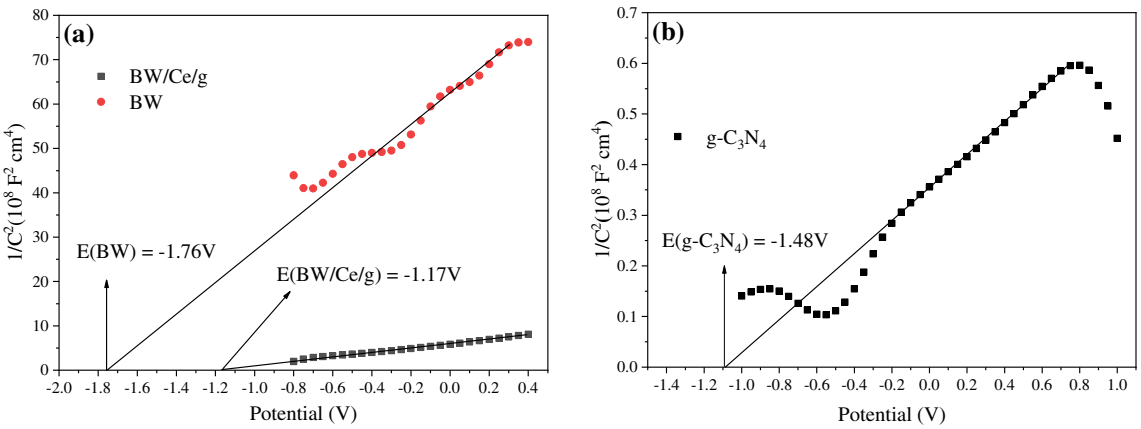

Fig. 8 Mott-Schottky curves of BW/Ce/g-3 and Bi_2WO_6(**a**), g-C_3N_4 (**b**)

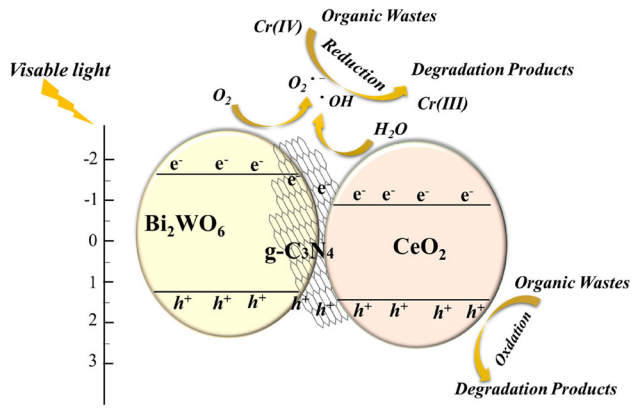

Scheme 1 Illustration of mechanism on charge separation of BW/Ce/g

Ce/g to possess better visible-light response ability. More than that, the great conductivity of g-C_3N_4 will be able to facilitate photogenerated electrons in the CB and holes in the VB to move fast in two opposite directions. In addition, the special energy level structure of the ternary heterojunctions can lengthen the migration path of photogenerated charge carriers, which will prolong the lives of photogenerated electrons and holes. This enabled more photogenerated electrons and holes were able to involve in photocatalytic reactions produce abundant free radicals, so that the photocatalytic activity of BW/Ce/g can be enhanced to degrade organic wastes and reduce Cr(VI).

4 Conclusion

Novel Ternary Bi_2WO_6/CeO_2/g-C_3N_4 composites were synthesized successfully in this study, which exhibited enhanced visible-light photocatalytic activity for oxidization of RhB and TH as well as reduction of Cr(VI). The characterization of the as-prepared composites demonstrated that Bi_2WO_6, CeO_2 and g-C_3N_4 were successfully coupled together to form the ternary heterojunctions structure, which can narrow the band gap of Bi_2WO_6/CeO_2/g-C_3N_4 to improve separation and migration of photogenerated electrons-hole pairs. Moreover, it has been indicated that the great conduction of g-C_3N_4 promoted the separation of photogenerated electron-holes pairs of B_2WO_6, in addition, the special ternary heterojunctions structure can lengthen the migration path of photogenerated charge carriers, which will prolong the lives of photogenerated electrons and holes. Therefore, Bi_2WO_6/CeO_2/g-C_3N_4 possessed enhanced photocatalytic activity. BW/Ce/g-3 can degrade 99.24% of RhB in 75 min, which was better than that of Bi_2WO_6 and Bi_2WO_6/CeO_2. More than that, BW/Ce/g exhibited enhanced photocatalytic activity for oxidation of TH (54.76%, 105 min) and reduction of Cr(VI) (94.85%,30 min). Meanwhile, the best synthesized condition was determined that the adding amount of CeO_2 was 0.043 g and g-C_3N_4 was 0.02 g. This study provided a novel photocatalyst for simultaneously effective degradation of organic wastewater and heavy metals wastewater, as well as that the feasibility of formation of ternary Bi_2WO_6/CeO_2/g-C_3N_4 composites with enhanced photocatalytic activity can be confirmed.

Acknowledgements

The present work was financially supported by Outstanding Young Talents Fund Project of Jilin Provincial Department of Science and Technology in 2019 (20190103109JH); National key research and development program (2017YFD0300405-4).

References

1. Z. Fang, Q. Li, L. Su, J. Chen, K.-C. Chou, X. Hou, Appl. Catal. B **241**, 548 (2019). https://doi.org/10.1016/j.apcatb.2018.09.074
2. X. Jiang, S. Lai, W. Xu et al., J. Alloys Compds. **809**, 151804 (2019). https://doi.org/10.1016/j.jallcom.2019.151804
3. I. Kretschmer, A.M. Senn, J.M. Meichtry et al., Appl. Catal. B **242**, 218 (2019). https://doi.org/10.1016/j.apcatb.2018.09.059
4. Y. Liu, J. Wang, P. Yang, RSC Adv. **6**, 34334 (2016). https://doi.org/10.1039/C6RA04430A
5. J. Wen, J. Xie, X. Chen, X. Li, Appl. Surf. Sci. **391**, 72 (2017). https://doi.org/10.1016/j.apsusc.2016.07.030
6. J. Yi, H. Mo, B. Zhang, J. Song, D. Liu, G. Zhuo, Sep. Purif. Technol. **211**, 474 (2019). https://doi.org/10.1016/j.seppur.2018.10.022
7. H. Yi, D. Huang, L. Qin et al., Appl. Catal. B **239**, 408 (2018). https://doi.org/10.1016/j.apcatb.2018.07.068
8. D. Lu, M. Yang, K.K. Kumar et al., Sep. Purif. Technol. **194**, 130 (2018). https://doi.org/10.1016/j.seppur.2017.11.039
9. Y. Qi, J. Ye, S. Zhang et al., J. Alloys Compds. **782**, 780 (2019). https://doi.org/10.1016/j.jallcom.2018.12.111

10. Q. Wang, Q. Lu, L. Yao, K. Sun, M. Wei, E. Guo, Dyes Pigm. **149**, 612 (2018). https://doi.org/10.1016/j.dyepig.2017.11.028
11. F. Zhang, S. Zou, T. Wang, Y. Shi, P. Liu, Photochem. Photobiol. **93**, 1154 (2017). https://doi.org/10.1111/php.12747
12. Z. Lv, H. Zhou, H. Liu, B. Liu, M. Liang, H. Guo, Chem. Eng. J. **330**, 1297 (2017). https://doi.org/10.1016/j.cej.2017.08.074
13. M. Liang, T. Borjigin, Y. Zhang, B. Liu, H. Liu, H. Guo, Appl. Catal. B **243**, 566 (2019). https://doi.org/10.1016/j.apcatb.2018.11.010
14. Q. Liang, J. Jin, M. Zhang et al., Appl. Catal. B **218**, 545 (2017). https://doi.org/10.1016/j.apcatb.2017.07.003
15. Y. Yang, J. Wu, T. Xiao et al., Appl. Catal. B (2019). https://doi.org/10.1016/j.apcatb.2019.117771
16. W.-K. Jo, S. Kumar, S. Eslava, S. Tonda, Appl. Catal. B **239**, 586 (2018). https://doi.org/10.1016/j.apcatb.2018.08.056
17. W. Mao, T. Wang, H. Wang, S. Zou, S. Liu, J. Mater. Sci. **29**, 15174 (2018). https://doi.org/10.1007/s10854-018-9659-y
18. Y. Zhao, X. Liang, Y. Wang et al., J. Colloid Interface Sci. **523**, 7 (2018). https://doi.org/10.1016/j.jcis.2018.03.078
19. X. Liu, L. He, X. Chen et al., Int. J. Hydrogen Energy **44**, 16154 (2019). https://doi.org/10.1016/j.ijhydene.2019.05.042
20. J. Rashid, N. Parveen, A. Iqbal et al., Sci. Rep. (2019). https://doi.org/10.1038/s41598-019-46544-7
21. J. Yu, C. Jiang, Q. Guan et al., Chemosphere **195**, 632 (2018). https://doi.org/10.1016/j.chemosphere.2017.12.128
22. T. Wang, W. Mao, Y. Wu et al., J. Mater. Sci. **30**, 16452 (2019). https://doi.org/10.1007/s10854-019-02021-5
23. H. Yi, M. Yan, D. Huang et al., Appl. Catal. B **250**, 52 (2019). https://doi.org/10.1016/j.apcatb.2019.03.008
24. D. Sun, D. Chi, Z. Yang et al., Int. J. Hydrogen Energy **44**, 16348 (2019). https://doi.org/10.1016/j.ijhydene.2019.04.275
25. A. Kumar, S.K. Sharma, G. Sharma et al., J. Hazard. Mater. **364**, 429 (2018). https://doi.org/10.1016/j.jhazmat.2018.10.060
26. M. Zargazi, M.H. Entezari, Appl. Catal. B **242**, 507 (2019). https://doi.org/10.1016/j.apcatb.2018.09.093
27. X. Lu, W. Che, X. Hu et al., Chem. Eng. J. **356**, 819 (2019). https://doi.org/10.1016/j.cej.2018.09.087
28. Y. Wang, X. Bai, F. Wang, S. Kang, C. Yin, X. Li, J. Hazard. Mater. **372**, 69 (2019). https://doi.org/10.1016/j.jhazmat.2017.10.007
29. H. Yang, B. Xu, S. Yuan, Q. Zhang, M. Zhang, T. Ohno, Appl. Catal. B **243**, 513 (2019). https://doi.org/10.1016/j.apcatb.2018.10.057
30. K. Selvakumar, A. Raja, M. Arunpandian, P. Rajasekaran, M. Swaminathan, Int. J. Environ. Anal. Chem. (2019). https://doi.org/10.1080/03067319.2019.1700968
31. J. Pan, Z. He, J. Su, R. Chen, B. Tang, Mater. Res. Express **6**, 115042 (2019). https://doi.org/10.1088/2053-1591/ab4666
32. X. Hu, W. Wang, G. Xie et al., Chemosphere **216**, 733 (2019). https://doi.org/10.1016/j.chemosphere.2018.10.181
33. Z.S. Seddigi, M.A. Gondal, S.G. Rashid, M.A. Abdulaziz, S.A. Ahmed, J. Mol. Catal. A **420**, 167 (2016). https://doi.org/10.1016/j.molcata.2016.04.026
34. F. Chen, D. Li, B. Luo, M. Chen, W. Shi, J. Alloys Compds. **694**, 193 (2017). https://doi.org/10.1016/j.jallcom.2016.09.326
35. M. Arif, M. Zhang, J. Yao et al., J. Alloys Compds. **792**, 878 (2019). https://doi.org/10.1016/j.jallcom.2019.03.321
36. S. Wang, H. Yang, X. Wang, W. Feng, J. Electron. Mater. **48**, 2067 (2019). https://doi.org/10.1007/s11664-019-07045-5
37. N. Tahmasebi, Z. Maleki, P. Farahnak, Mater. Sci. Semicond. Process. **89**, 32 (2019). https://doi.org/10.1016/j.mssp.2018.08.026
38. Q. Liang, J. Jin, C. Liu et al., J. Mater. Sci. **28**, 11279 (2017). https://doi.org/10.1007/s10854-017-6918-2
39. T. Wang, S. Liu, W. Mao et al., J. Hazard. Mater. **389**, 121827 (2020). https://doi.org/10.1016/j.jhazmat.2019.121827
40. Z. Zhu, W. Fan, Z. Liu et al., J. Photochem. Photobiol A **358**, 284 (2018). https://doi.org/10.1016/j.jphotochem.2018.03.027
41. Y. Wang, W. Jiang, W. Luo, X. Chen, Y. Zhu, Appl. Catal. B **237**, 633 (2018). https://doi.org/10.1016/j.apcatb.2018.06.013
42. G. Swain, S. Sultana, J. Moma, K. Parida, Inorg. Chem. **57**, 10059 (2018). https://doi.org/10.1021/acs.inorgchem.8b01221
43. R. Tao, C. Shao, X. Li et al., J. Colloid Interface Sci. **529**, 404 (2018). https://doi.org/10.1016/j.jcis.2018.06.035
44. H. Yu, J. Xu, C. Yin, Z. Liu, Y. Li, J. Solid State Chem. **272**, 102 (2019). https://doi.org/10.1016/j.jssc.2019.01.021